American Mineralogist, Volume 78, pages 1002–1015, 1993

Synthesis and stability of $Fe_3^{2+}Fe_2^{3+}Si_3O_{12}$ garnet and phase relations with $Fe_3Al_2Si_3O_{12}$-$Fe_3^{2+}Fe_2^{3+}Si_3O_{12}$ solutions

ALAN B. WOODLAND, HUGH ST.C. O'NEILL
Bayerisches Geoinstitut, Postfach 10 12 51, D-95440 Bayreuth, Germany

ABSTRACT

Garnets containing both Fe^{2+} and Fe^{3+} are potentially useful monitors of f_{O_2} in metamorphic rocks and garnet peridotites of the mantle. However, little is known about the properties or stability of such garnets. We have synthesized end-member $Fe_3^{2+}Fe_2^{3+}Si_3O_{12}$ garnet and garnet along the almandine ($Fe_3^{2+}Al_2Si_3O_{12}$)–$Fe_3^{2+}Fe_2^{3+}Si_3O_{12}$ join, where Al and Fe^{3+} mix on the octahedral sites. The experiments were performed with a series of glasses and slags with a fixed ratio of Fe^{3+}/Fe_{tot} in a piston cylinder apparatus and a multianvil press using Ag as the capsule material. The extent of Fe^{3+} substitution for Al is strongly pressure dependent. At 1100 °C, the maximum $Fe_3^{2+}Fe_2^{3+}Si_3O_{12}$ content is 13, 43, and 75 mol% at 2.7, 6.5, and 8.0 GPa, respectively. The end-member ferrous-ferric garnet is only stable at pressures above ≈9.3 GPa. However, skiagite becomes unstable at higher pressures of even <13.0 GPa. Mössbauer spectroscopy confirms that Fe^{2+} and Fe^{3+} are restricted to the dodecahedral and octahedral sites, respectively. Molar volumes of $Fe_3^{2+}Fe_2^{3+}Si_3O_{12}$ and almandine are 121.44 ± 0.01 cm³ [$a_0 = 11.7278(6)$ Å] and 115.23 ± 0.01 cm³, [$a_0 = 11.5244(4)$ Å] and vary linearly across the binary join.

At 1100 °C, the equilibrium garnet solid solutions coexist with fayalite + spinel + quartz at $P < 1.6$ GPa, with spinel + $Fe_2Si_2O_6$ + quartz or coesite at $1.6 < P < 5.0$ GPa, and with Si-rich spinel + coesite or stishovite above 5.0 GPa. The coexisting spinel and pyroxene are very Al poor, indicating that Al is strongly partitioned into the garnet. Based upon Al-Fe^{3+} exchange between garnet and spinel, a $\Delta_f G^\circ_{1,1373} = -2975.2 \pm 3.0$ kJ/mol is obtained for $Fe_3^{2+}Fe_2^{3+}Si_3O_{12}$, assuming ideal mixing in the garnet. The spinel becomes increasingly Fe_2SiO_4-rich with increasing pressure such that the Fe^{3+}/Fe_{tot} of the end-member $Fe_3^{2+}Fe_2^{3+}Si_3O_{12}$ garnet and coexisting spinel are nearly the same.

INTRODUCTION

Garnet is an important phase in the Earth's lower crust and mantle. Its common occurrence has led to the use of garnet-bearing equilibria as indicators of temperature and pressure (e.g., O'Neill and Wood, 1979; Bohlen et al., 1983b; Hackler and Wood, 1989). The compositions of such garnets can generally be expressed in terms of three main components: pyrope ($Mg_3Al_2Si_3O_{12}$), grossular ($Ca_3Al_2Si_3O_{12}$), and almandine ($Fe_3^{2+}Al_2Si_3O_{12}$). The presence of Fe implies that the stability of garnet is controlled in part by f_{O_2}. The incorporation of Fe^{3+} in aluminous garnet has several important petrologic implications. Garnet-bearing reactions could be potential monitors of f_{O_2} for garnet peridotites and eclogites (Luth et al., 1990). Garnet could be an important sink for Fe^{3+} at depths >≈60 km, where Fe^{3+}-bearing aluminous spinel becomes unstable (Wood et al., 1990). The incorporation of Fe^{3+} in majorite garnet [$(Mg,Fe^{2+})_4Si_4O_{12}$] could strongly influence the f_{O_2} in the transition zone of the mantle (O'Neill et al., 1993). The presence of Fe^{3+} in garnet can also have a significant effect on temperature and pressure estimates, especially those based upon Mg-Fe exchange equilibria (Luth et al., 1990).

Woodland and Wood (1989) derived the free energy of formation of almandine from the reaction involving sillimanite, quartz, and metallic Fe. Their study revealed that small amounts of Fe^{3+} could substitute for Al and that these small quantities had an apparent effect on garnet stability. Minor substitution of Fe^{3+} for Al in almandine was also reported by Geiger et al. (1987). The recent study of mantle-derived garnets by Luth et al. (1990) showed that up to 12% of the Fe can be in the ferric state. Their attempt at using the Fe^{3+} content of the garnets to determine f_{O_2} was hampered, however, by the absence of thermochemical data on the mixing properties of Fe^{3+} in garnet. Mössbauer spectroscopy on these and other garnets (Amthauer et al., 1976) indicates that Fe^{3+} usually resides on the octahedral sites. Therefore, the Fe^{3+}-bearing components to consider are skiagite ($Fe_3^{2+}Fe_2^{3+}Si_3O_{12}$), khoharite ($Mg_3Fe_2^{3+}Si_3O_{12}$), and andradite ($Ca_3Fe_2^{3+}Si_3O_{12}$). Thermochemical data for all three components are necessary in order to account for the reciprocal solid-solution effects in natural multicomponent $(Mg,Fe^{2+},Ca)_3(Al,Cr,Fe^{3+})_2Si_3O_{12}$ garnet solid solutions. $Fe_3^{2+}Fe_2^{3+}Si_3O_{12}$ is the obvious choice for a study of garnets that contain both Fe^{2+} and Fe^{3+}, since cation mixing can be limited to one site. In $Fe_3Al_2Si_3O_{12}$-$Fe_3^{2+}Fe_2^{3+}Si_3O_{12}$ solutions, Fe^{3+} substitutes for Al on the octahedral sites. Although skiagite,

0003–004X/93/0910–1002$02.00

the name for $Fe_3^{2+}Fe_2^{3+}Si_3O_{12}$, has been discredited as a proper mineral name, we retain the use of the term skiagite (ski) to refer to an end-member component that may occur in complex garnet solid solutions.

Garnet with significant skiagite content has been synthesized by Schreyer and Baller (1980) and Lattard and Schreyer (1983) in the Mn-Fe-Si-O system. Synthesis of the pure skiagite end-member was first reported by Karpinskaya et al. (1982), based upon several X-ray reflections that could not be assigned to the other phases present in their experimental products. Their experiments suggest that garnet could be a stable phase in the system $FeO-Fe_2O_3-SiO_2$ at high pressure.

The purpose of this study was to determine the maximum extent of Fe^{3+} substitution for Al in garnet by the synthesis of almandine-skiagite solid solutions. The synthesis of the skiagite end-member was also important to verify the results of Karpinskaya et al. (1982) and to characterize this end-member garnet. In addition, we set out to establish the phase relations between garnet and spinel, olivine, and pyroxene in the system $FeO-FeO_{1.5}-AlO_{1.5}-SiO_2$ and to derive some thermodynamic properties of skiagite and almandine-skiagite solutions.

EXPERIMENTAL METHODS

Apparatus and experimental techniques

Experiments in the pressure range of 1.5–5.0 GPa were conducted in a piston cylinder apparatus. Talc-Pyrex pressure cells with diameters of 1.905 and 1.270 cm were used, depending on the desired pressure. The temperature was controlled by means of $Pt-Pt_{90}Rh_{10}$ thermocouples with no correction for the effect of pressure on the emf. The experiments employed the piston-in technique. The pressure was calibrated in the 1.905-cm cells from (1) the olivine-spinel transition in Mg_2GeO_4 (Ross and Navrotsky, 1987), (2) the albite + jadeite + quartz equilibrium (Holland, 1980), (3) the ferrosilite + fayalite + quartz equilibrium (Bohlen et al., 1980), and (4) the pyroxene-garnet transition in $CaGeO_3$ (Ross et al., 1986). The pressure calibration for the 1.270-cm cells was determined from (1) the quartz-coesite transition (Bohlen and Boettcher, 1982), and (2) the olivine-spinel transition in Mg_2GeO_4. The uncertainty in pressure is estimated to be $\approx$0.1 GPa, based upon the width of our calibration brackets. The duration of the experiments was mostly between 40 and 100 h. The starting materials were ground under acetone and packed in 5-mm Ag capsules with walls 0.5 mm thick and sealed by friction-fitting lids hammered in place. The choice of Ag as the capsule material was based on the premise that Ag would not absorb any Fe (Massalski et al., 1986) and that Ag is one of the metals more impervious to H_2. This is an important consideration, since diffusion of H_2 into the capsule during the experiment could change the O content of the solid and, therefore, the Fe^{3+}/Fe_{tot} ratio of the sample. Experiments involving almandine-rich compositions ($\leq ski_{05}$) were conducted in 6-mm graphite capsules. Most experiments were conducted at 1100 °C; however, below $\approx$3.0 GPa the experiments were at a somewhat lower temperature to avoid melting of the Ag capsules. Several experiments at low pressure were performed with Au capsules in order to reach 1100 °C without melting the capsule material. It is possible that some Fe loss to the capsule could have occurred in these experiments, since there is significant Fe solubility in Au.

Experiments at 5.5–10.0 GPa were conducted in the Sumitomo 1200 multianvil press at the Bayerisches Geoinstitut using Toshiba F grade tungsten carbide cubes with an 11-mm truncated edge. The pressure cells were Cr_2O_3-doped MgO octahedra, 18 mm on an edge, heated by a graphite resistance heater. Temperature was monitored by axially inserted $Pt-Pt_{90}Rh_{10}$ thermocouples with no correction made for the pressure effect on emf. The pressure was calibrated at room temperature using the transitions in Bi (I-II, III-V) and at 1000 and 1450 °C using the transitions (1) quartz-coesite (Bohlen and Boettcher, 1982), (2) coesite-stishovite (Yagi and Akimoto, 1976), and (3) fayalite–γ spinel (Yagi et al., 1987). The accuracy in the pressure is estimated to be $\pm$0.3 GPa, based on the width of the reversal brackets and repeated checks of these reactions. The capsules for the multianvil press experiments were made from 1.7-mm Ag tubing. The ends were sealed by the insertion of an Ag disk, followed by crimping and hammering, which produced a cold weld. The duration of the multianvil experiments was 10–14.5 h.

Starting materials

Since control of f_{O_2} (e.g., by the double capsule technique) is impractical in the multianvil experiments, we chose instead to rely on a closed system approach for experiments in both apparatus by analysis of the Fe^{3+}/Fe_{tot} ratio in the products. In order to obtain starting materials with the correct stoichiometry for the garnet solid solutions, the Fe^{3+}/Fe_{tot} ratio must be set. The Fe^{3+}/Fe_{tot} ratio varies from 0.0 in almandine (only Fe^{2+} is present) to 0.40 for pure skiagite. This ratio was established by using mixtures of fayalite, quartz, and an appropriate hercynite-magnetite solid solution to achieve the correct Fe^{3+}/Fe_{tot}. Although this proved effective for the synthesis of the almandine end-member using pure hercynite, the syntheses of the solid solutions were not successful. In the experiments with alm-ski solutions, almandine-rich garnet would nucleate on and mantle the spinel, effectively stopping the reaction from proceeding to completion. In addition, local Al-Fe exchange would occur between the garnet and the spinel, yielding a very almandine-rich garnet and magnetite-rich rims on the spinel grains. To circumvent this problem, glasses or slags were prepared by melting stoichiometric amounts of Fe_2O_3, Al_2O_3, and SiO_2 at 1500 °C. The correct Fe^{3+}/Fe_{tot} ratio was achieved by controlling the f_{O_2} of the furnace atmosphere using $CO-CO_2$ or $Ar-O_2$ gas mixes. The value of f_{O_2} that would yield the desired Fe^{3+}/Fe_{tot} was estimated from Kress and Carmichael (1988) and from Figure 6902 in Roth et al. (1987, p. 454–456). Nonmagnetic glasses

TABLE 1. Experimental results

							Cell edge (Å)		Spinel comp.		
Expt.	T (°C)	P (GPa)	t (h)	Intended comp.	Phases produced	Probe comp.	Garnet	Spinel	Fe_2SiO_4	Mt	Hc
al5*	1100	1.5	6	ski_{00}	gt	ski_{00}	11.531(2)				
aw1*,**	1200	2.0	42	ski_{00}	gt + q + Fe	ski_{00}	11.5285(2)				
aw6*,**	1200	1.9	44	ski_{00}	gt + q + Fe	ski_{00}	11.5285(2)				
aw14*,**	1100	1.7	24	ski_{00}	gt	ski_{02}	11.5312(8)				
aw35**	1000	2.0	168	ski_{00}	gt + opx + q	ski_{00}	11.5292(7)				
aw43**	1080	3.2	41	ski_{00}	gt + opx	ski_{02}	11.5333(2)				
aw18*	1200	3.0	24	ski_{05}	gt + q	ski_{02}	11.5299(5)				
aw25	1080	2.7	46	ski_{10}	gt + q	ski_{08}	11.5400(6)				
aw26	1080	2.7	96	ski_{10}	gt + q	ski_{08}	11.5390(9)				
aw30	1080	2.7	97	ski_{10}	gt + q	ski_{07}	11.5408(3)				
aw31	1030	1.9	96	ski_{10}	gt + q + sp	ski_{09}	11.5380(2)	8.369(1)	4	87	9.0
aw45	1080	2.7	101	ski_{10}	gt + q	ski_{08}	11.5405(2)				
aw21	1100	3.0	40	ski_{15}	gt + sp + q + opx	ski_{12}	11.5494(2)	8.373(1)	7	88	5.3
aw29	1080	2.7	89	ski_{15}	gt + sp + q + opx	ski_{12}	11.5495(2)	8.374(1)	7	88	4.8
aw37	1100	4.0	96	ski_{15}	gt	ski_{15}	11.5546(4)				
aw41	1100	3.5	89.5	ski_{15}	gt + sp	ski_{17}	11.5594(2)	8.377(1)			
aw48†	1100	1.7	116.5	ski_{15}	gt + sp + q + opx	ski_{10}	11.5426(5)	8.360(1)	4	83	13.0
aw15*	1200	3.0	95	ski_{20}	gt + sp + q + opx	ski_{03}	11.5336(5)				
aw21	1100	3.0	40	ski_{20}	gt + sp + q + opx	ski_{13}	11.5522(6)	8.371(1)	7	88	5.3
aw26	1080	2.7	96	ski_{20}	gt + opx + fa	ski_{11}	11.5477(7)				
aw29	1080	2.7	89	ski_{20}	gt + sp + q + opx	ski_{12}	11.5501(2)	8.374(1)	8	87	5.0
aw32	1080	2.7	90	ski_{20}	gt + sp + q + opx	ski_{13}	11.5507(10)		8	87	5.2
aw34†	1180	2.7	49	ski_{20}	gt + opx + q	ski_{09}	11.5430(4)				
aw37	1100	4.0	96	ski_{20}	gt	ski_{21}	11.5571(5)				
aw23	1080	2.7	47	ski_{30}	gt + sp + q + opx	ski_{13}	11.5489(2)	8.368(1)	10	85	5.2
aw38	1100	4.4	70	ski_{30}	gt + sp + coe	ski_{18}	11.5647(5)	8.373(1)	10	87	3.0
aw47	1100	4.8	46	ski_{30}	gt + sp + q + opx	ski_{30}	11.5837(7)				
uhp458	1100	6.0	11	ski_{30}	gt + coe + sp	ski_{29}	11.5777(7)	8.359(1)			
uhp541	1100	6.5	12	ski_{40}	gt	ski_{41}	11.6061(9)				
uhp541	1100	6.5	12	ski_{50}	gt + sp + opx	ski_{44}	11.6123(8)				
uhp627	1100	7.0	12.5	ski_{50}	gt + coe + sp	ski_{50}	11.6273(3)				
uhp532	1100	8.0	12	ski_{70}	gt + sp + cpx	ski_{70}	11.6615(4)		63	36	0.8
uhp497	1100	9.0	12	ski_{80}	gt + hem + coe	ski_{79}	11.6841(7)				
uhp532	1100	8.0	12	ski_{80}	gt + coe + sp	ski_{75}	11.6735(4)	8.3242(8)	46	54	0.4
uhp610	1100	8.5	12	ski_{80}	gt + sp + coe	ski_{76}	11.6818(3)	8.3252(15)	44	56	0.3
uhp589	1100	9.0	12	ski_{90}	gt + sp + hem + coe	ski_{77}	11.6840(4)	8.3523(4)			
uhp598	1100	9.5	14	ski_{90}	gt + sp + hem + coe	ski_{90}	11.7076(7)				
uhp524	1100	9.0	11	ski_{100}	gt + sp + coe	ski_{82}	11.6903(7)	8.3153(9)	45	55	0.2
uhp548	1100	10.0	12	ski_{100}	sp + gt + st	ski_{100}	11.7286(10)	8.3187(2)	39	61	
uhp548	1100	10.0	12	ski_{100}	sp + gt + st	ski_{100}	11.7273(4)	8.3133(3)	45	55	
uhp598	1100	9.5	14	ski_{100}‡	sp + coe + hem + gt	ski_{100}	11.726(20)	8.3187(10)	43	57	
uhp666**	1100	9.3	12.5	ski_{100}‡	sp + coe + gt + (px)		11.7250(15)	8.3224(2)	36	64	
uhp693**	1100	10.5	11.6	ski_{100}‡	sp + gt + st	ski_{95}	11.7163(5)	8.2981(14)			
uhp702**	1100	9.7	12.5	ski_{100}‡	gt + st + sp	ski_{100}	11.7272(7)				
uhp636**	1100	10.0	12.5	$\text{ski}_{60}\text{-fm}_{40}$	gt + sp + st + (px)	ski_{98}	11.7254(4)	8.2629(6)	76	24	
uhp693**	1100	10.5	11.6	$\text{ski}_{60}\text{-fm}_{40}$	sp + st + gt		11.7126(8)	8.2649(8)	74	26	

Reequilibration experiments

							Cell edge (Å)		Spinel comp.		
Expt.	T (°C)	P (GPa)	t (h)	Starting comp.	Phases produced	Probe comp.	Garnet	Spinel	Fe_2SiO_4	Mt	Hc
aw45	1080	2.7	101	ski_{30}r	2gt + sp + opx + q	ski_{13}	11.5510(10)	8.3745(2)	10	85	5.2
uhp642	1100	5.5	13.5	ski_{50}r	2gt + sp + coe + opx	ski_{33}	11.5909(2)	8.370(3)	20	78	1.8
uhp627	1100	7.0	12.5	ski_{80}r	2gt + sp + coe + opx	ski_{59}	11.6430(12)	8.347(3)	32	68	0.9
aw69	1100	4.1	115	ski_{13}r	gt + px + sp + coe	ski_{19}					
uhp835	1100	6.0	14.5	ski_{21}r	gt + px + sp + coe	ski_{35}					

Note: (px) = unreacted starting material.
* Used graphite capsule.
** Oxide mix.
† Used Au capsule.
‡ Garnet seed added.

were obtained up to compositions of 70 mol% almandine and 30 mol% skiagite (ski_{30}). However, at more Fe-rich compositions, quenching a glass became increasingly difficult, and a magnetic vitreous slag resulted. The Fe^{3+}/Fe_{tot} ratios of the glasses were checked by wet chemistry and were found to be within 10% of the nominal values. The glasses were also checked by Mössbauer spectroscopy. The resulting Fe^{3+}/Fe_{tot} values were found to be sensitive to the scheme used for fitting the spectra, but the range in values obtained was in agreement with the nominal ratio. The slags were not checked by either method because of the difficulty in completely dissolving oxide phases without causing oxidation and therefore spuriously high Fe^{3+} contents (Lucas et al., 1989) and because the presence of multiple phases would make any Mössbauer spectrum virtually impossible to interpret in a quantitative fashion. Since several of the slag starting materials produced homogeneous garnets either as a single phase or with only a trace of additional phases, the actual Fe^{3+}/Fe_{tot} of the slags must have been close to the intended values (see below).

Several starting materials were used in experiments in the FeO-$FeO_{1.5}$-SiO_2 subsystem. Slags were synthesized in the manner described above. We also used two mineral mixes, ferrosilite + hematite and magnetite + fayalite + SiO_2. The ferrosilite was synthesized from a mixture of fayalite and quartz in a piston cylinder apparatus at 1000 °C and 1.8 GPa. It was then ground together with hematite to produce a skiagite bulk composition. A stoichiometric mixture of fayalite, magnetite, and either very high purity silica glass or SiO_2 produced from gel was also used. These mixtures were less successful in terms of yield, apparently owing to the sluggishness of reaction between SiO_2 and spinel.

Experimental products and analytical methods

The products were analyzed by X-ray diffraction, electron microprobe, and Mössbauer spectroscopy. The experimental conditions and the phases produced are listed in Table 1. The cell edges of the garnets were determined from the average of at least ten peaks above 60° 2θ using Ge monochromated $CoK\alpha_1$ radiation and NBS Si metal as an internal standard (STOE STADIP focusing diffractometer in transmission mode). Phase compositions were determined using a Cameca Camebax SX50 microprobe in wavelength-dispersive mode with a 15-kV accelerating voltage and a 15-nA beam current. The standards were Fe_2O_3 for Fe, spinel for Al, and either andradite or orthoclase for Si. The raw counts were recalculated using the PAP correction procedure. Garnet compositions were calculated assuming ideal stoichiometry of 8 cations pfu and charge balance.

Resonant absorption spectra were collected at 298 K with a Mössbauer spectrometer operating in constant acceleration mode and a ≈50 mCi ^{57}Co in Rh source. The velocity ramp was ±5 mm/s. Mirror-image spectra were collected over 512 channels and calibrated with respect to α Fe at room temperature. The samples were prepared so that the Fe concentration was between 3 and 5 mg/cm^2 to avoid effects from saturation. The spectra were fitted using the PC-MOS software obtained from CMTE Elektronik, Auenstraße 15, D-85521 Riemerling, Germany. Some spectra were also fitted using the Mossfita program (see Luth et al., 1990) and were found to give the same hyperfine parameters and area ratios within the uncertainties of ±0.01 mm/s and ±0.01, respectively.

RESULTS AND DISCUSSION

Garnet occurs as a single phase or coexists with one or more additional phases. The results of the individual experiments are summarized in Table 1. All the garnets are optically isotropic. Under oils the almandine-rich samples with compositions ≤5 mol% skiagite are greenish. With increasing Fe^{3+} content, the garnets become pinkish ($\approx X_{ski} \leq 30$) and then take on a dark red-brown color. The skiagite end-member is dark red-brown. The grain size is variable, with some samples having euhedral crystals up to 150 μm across. Other samples have much finer grained garnets, on the order of 5–30 μm. The grain size of the coexisting phases is often much smaller than that of the garnet. In some instances the nongarnet phases are <3 μm across, precluding quantitative microprobe analysis.

Garnet composition

The almandine mole fraction was determined from the Al content as measured by electron microprobe, and the Fe^{3+} content was then calculated assuming ideal stoichiometry. Representative analyses of the garnets and associated phases are given in Table 2. The garnets in the experiments were quite homogeneous, generally yielding standard deviations of ≤2 mol%, corresponding to uncertainties in the calculated Fe^{3+}/Fe_{tot} of ≤0.013. However, the presence of both Fe^{2+} and Fe^{3+} adds to analytical uncertainty. For a garnet to lie on the almandine-skiagite binary also requires that Fe^{2+} and Fe^{3+} be restricted to the dodecahedral and octahedral sites, respectively. Otherwise, some other garnet component such as $Fe_4^{2+}Si_4O_{12}$ must be considered.

To address this problem, Mössbauer spectra were collected from samples that either were single phase or contained only a trace of additional phases. The resultant room-temperature hyperfine parameters are listed in Table 3. Representative room-temperature Mössbauer spectra of four garnet samples with increasing Fe^{3+} content are presented in Figure 1a–1d. The most obvious features are the two doublets with distinctive line positions. The doublet with a large quadrupole splitting (QS) of ≈3.5 mm/s and an isomer shift (IS) of 1.3 mm/s is characteristic of Fe^{2+} in dodecahedral coordination (Amthauer et al., 1976). No statistically significant asymmetry is apparent between the low and high velocity peaks, as is often observed in garnets (e.g., Luth et al., 1990; Amthauer et al., 1976). When the two peaks are fitted separately rather than as a constrained doublet, the peak widths are identical within the resolution of the spectra. The full peak widths at half maximum (FWHM) for the $^{[8]}Fe^{2+}$ were 0.23–0.29 mm/s (Table 3). The other doublet, with a QS of 0.20–0.25 mm/s and IS of 0.31–0.36 mm/s, grows in relative intensity with increasing skiagite content and can therefore be assigned to Fe^{3+}. The coordination of the Fe^{3+} can be deduced by comparison with the ranges in hyperfine parameters for $^{[6]}Fe^{3+}$ and $^{[4]}Fe^{3+}$ in garnet samples given by Amthauer et al. (1976): $^{[6]}Fe^{3+}$, IS =

TABLE 2. Representative microprobe analyses of synthesized garnet samples and associated phases

Expt.	aw1 (ski$_{00}$)	aw6 (ski$_{00}$)	aw14 (ski$_{02}$)	aw43 (ski$_{02}$)	aw18 (ski$_{05}$)	aw25 (ski$_{10}$)
Phase	Gt	Gt	Gt	Gt	Gt	Gt
Al_2O_3	20.43	20.33	20.06	19.90	19.88	18.89
FeO_{tot}	43.48	43.51	43.57	43.72	43.20	45.65
SiO_2	35.91	35.85	35.90	35.64	35.58	36.42
Total	99.82	99.69	99.53	99.26	98.66	100.96
Structural formula						
Al	1.999	1.993	1.971	1.962	1.970	1.839
Fe^{2+}	2.982	2.981	2.992	2.981	2.992	3.008
Fe^{3+}	0.038	0.044	0.045	0.077	0.046	0.145
Si	2.982	2.981	2.992	2.981	2.992	3.008

Expt.	aw26 (ski$_{10}$)	aw30 (ski$_{10}$)	aw31 (ski$_{10}$)	aw31 (ski$_{10}$)	aw45 (ski$_{10}$)	aw21 (ski$_{15}$)
Phase	Gt	Gt	Gt	Sp	Gt	Gt
Al_2O_3	18.75	19.11	18.50	4.32	18.66	17.56
FeO_{tot}	44.64	45.49	45.13	88.47	45.51	46.41
SiO_2	36.39	36.29	36.12	1.01	36.10	35.87
Total	99.78	100.89	99.75	93.80	100.27	99.84
Structural formula						
Al	1.845	1.860	1.823	0.096	1.830	1.736
Fe^{2+}	3.038	2.997	3.021	1.038	3.004	3.009
Fe^{3+}	0.079	0.145	0.136	1.734	0.163	0.247
Si	3.038	2.997	3.021	0.038	3.004	3.009

Expt.	aw21 (ski$_{15}$)	aw21 (ski$_{15}$)	aw29 (ski$_{15}$)	aw29 (ski$_{15}$)	aw29 (ski$_{15}$)	aw31 (ski$_{15}$)
Phase	Sp	Px	Gt	Sp	Px	Gt
Al_2O_3	2.35	1.71	17.78	2.10	1.65	18.43
FeO_{tot}	89.74	54.41	46.44	88.25	54.04	45.34
SiO_2	1.85	42.06	35.70	1.93	43.53	35.70
Total	93.94	98.18	99.92	92.28	99.22	99.47
Structural formula						
Al	0.104	0.091	1.756	0.095	0.086	1.823
Fe^{2+}	1.070	2.048	2.991	1.074	2.001	2.996
Fe^{3+}	1.756		0.263	1.757		0.186
Si	0.070	1.893	2.991	0.074	1.928	2.996

Expt.	aw31 (ski$_{15}$)	aw37 (ski$_{15}$)	aw41 (ski$_{15}$)	aw41 (ski$_{15}$)	aw48 (ski$_{15}$)	aw48 (ski$_{15}$)
Phase	Sp	Gt	Gt	Sp	Gt	Sp
Al_2O_3	3.76	17.07	16.86	1.78	18.27	5.95
FeO_{tot}	87.86	46.57	47.61	90.09	45.46	87.99
SiO_2	1.18	35.55	35.60	1.94	35.88	1.23
Total	92.80	99.19	100.07	93.81	99.69	95.17
Structural formula						
Al	0.168	1.701	1.668	0.079	1.805	0.257
Fe^{2+}	1.045	3.006	2.989	1.073	3.008	1.045
Fe^{3+}	1.742	0.287	0.354	1.774	0.179	1.653
Si	0.045	3.006	2.989	0.073	3.008	0.045

Expt.	aw15 (ski$_{20}$)	aw15 (ski$_{20}$)	aw21 (ski$_{20}$)	aw21 (ski$_{20}$)	aw21 (ski$_{20}$)	aw26 (ski$_{20}$)
Phase	Gt	Px	Gt	Sp	Px	Gt
Al_2O_3	19.67	5.40	17.53	2.36	1.71	17.87
FeO_{tot}	43.96	50.84	47.07	89.41	54.41	45.76
SiO_2	35.43	41.22	35.90	1.92	42.06	35.69
Total	99.06	97.46	100.50	93.69	98.18	99.32
Structural formula						
Al	1.945	0.283	1.723	0.105	0.091	1.773
Fe^{2+}	2.972	1.893	2.994	1.072	2.048	3.005
Fe^{3+}	0.112		0.289	1.750		0.217
Si	2.972	1.835	2.994	0.072	1.893	3.005

TABLE 2.—*Continued*

Expt.	aw26 (ski$_{20}$)	aw26 (ski$_{20}$)	aw29 (ski$_{20}$)	aw29 (ski$_{20}$)	aw29 (ski$_{20}$)	aw32 (ski$_{20}$)
Phase	Px	Fa	Gt	Sp	Px	Gt
Al_2O_3	0.97		17.91	2.30	1.44	17.26
FeO_{tot}	53.85	69.54	46.52	88.63	53.90	46.25
SiO_2	44.41	29.49	35.98	1.96	43.68	35.91
Total	99.23	99.03	100.41	92.89	99.02	99.42
Structural formula						
Al	0.051		1.759	0.103	0.075	1.714
Fe^{2+}	1.991	1.985	2.999	1.075	1.999	3.026
Fe^{3+}			0.244	1.748		0.233
Si	1.964	1.006	2.999	0.075	1.938	3.026

Expt.	aw32 (ski$_{20}$)	aw32 (ski$_{20}$)	aw34 (ski$_{20}$)	aw34 (ski$_{20}$)	aw37 (ski$_{20}$)	aw23 (ski$_{30}$)
Phase	Sp	Px	Gt	Px	Gt	Gt
Al_2O_3	2.19	1.49	18.40	3.58	16.04	17.91
FeO_{tot}	87.18	53.51	45.41	52.59	48.49	46.97
SiO_2	1.86	43.56	35.45	42.09	35.79	36.29
Total	91.23	98.56	99.26	98.26	100.32	101.17
Structural formula						
Al	0.100	0.078	1.824	0.187	1.588	1.747
Fe^{2+}	1.072	1.993	2.892	1.956	3.006	3.003
Fe^{3+}	1.756		0.212		0.400	0.247
Si	0.072	1.940	2.892	1.872	3.006	3.003

Expt.	aw23 (ski$_{30}$)	aw23 (ski$_{30}$)	aw38 (ski$_{30}$)	aw38 (ski$_{30}$)	u458 (ski$_{70}$)	u642 (ski$_{30}$)
Phase	Sp	Px	Gt	Sp	Gt	Gt
Al_2O_3	2.34	1.24	16.53	1.36	13.92	14.16
FeO_{tot}	89.34	54.00	47.46	89.36	49.90	50.93
SiO_2	2.74	43.85	35.56	2.59	34.44	35.46
Total	94.42	99.09	99.58	93.31	98.26	100.55
Structural formula						
Al	0.103	0.065	1.645	0.061	1.418	1.409
Fe^{2+}	1.102	2.003	3.002	1.098	2.976	2.994
Fe^{3+}	1.692		0.351	1.742	0.630	0.602
Si	0.102	1.944	3.002	0.098	2.976	2.994

Expt.	u642 (ski$_{30}$)	u541 (ski$_{40}$)	u541 (ski$_{50}$)	u627 (ski$_{50}$)	u532 (ski$_{70}$)	u532 (ski$_{70}$)
Phase	Sp	Gt	Gt	Gt	Gt	Gt
Al_2O_3	0.73	11.40	10.43	9.93	5.54	0.35
FeO_{tot}	89.71	51.93	52.89	54.17	57.75	76.99
SiO_2	2.79	34.17	34.68	34.41	33.45	17.24
Total	93.23	97.50	98.00	98.51	96.74	94.58
Structural formula						
Al	0.033	1.181	1.078	1.024	0.592	0.015
Fe^{2+}	1.107	3.003	3.042	3.011	3.031	1.630
Fe^{3+}	1.754	0.814	0.838	0.953	1.345	0.724
Si	0.106	3.003	3.042	3.011	3.031	0.630

Expt.	u497 (ski$_{80}$)	u532 (ski$_{80}$)	u532 (ski$_{80}$)	u610 (ski$_{80}$)	u610 (ski$_{80}$)	u589 (ski$_{90}$)
Phase	Gt	Gt	Sp	Gt	Sp	Gt
Al_2O_3	4.05	4.58	0.19	4.47	0.13	4.46
FeO_{tot}	60.76	59.49	76.79	59.37	81.19	59.98
SiO_2	33.21	32.92	12.31	33.06	11.49	33.05
Total	98.02	96.99	92.29	96.80	92.81	97.49
Structural formula						
Al	0.430	0.490	0.008	0.479	0.006	0.475
Fe^{2+}	2.992	2.991	1.466	3.006	1.433	2.989
Fe^{3+}	1.586	1.529	1.060	0.754	1.128	1.547
Si	2.992	2.991	0.466	3.006	0.433	2.989

TABLE 2.—*Continued*

Expt.	u598 (ski$_{90}$)	u524 (sk$_{100}$)	u524 (sk$_{100}$)	u548 (sk$_{100}$)	u548 (sk$_{100}$)	u548 (sk$_{100}$)
Phase	Gt	Gt	Sp	Gt	Sp	Gt
Al_2O_3	1.94	3.27	0.09			
FeO_{tot}	62.72	61.72	82.70	63.29	83.70	63.85
SiO_2	32.66	33.46	12.21	32.01	10.48	33.23
Total	97.32	98.45	95.00	95.30	94.25	97.08
Structural formula						
Al	0.209	0.347	0.004			
Fe^{2+}	2.990	3.010	1.450	3.015	1.391	3.069
Fe^{3+}	1.812	1.633	1.097	1.97	1.219	1.862
Si	2.990	3.010	0.450	3.015	0.391	3.069

Expt.	u548 (sk$_{100}$)	u598 (sk$_{100}$)	u636 (sk$_{100}$)	u636 (sk$_{100}$)	u666 (sk$_{100}$)	u666 (sk$_{100}$)
Phase	Sp	Sp	Gt	Sp	Gt	Sp
Al_2O_3			0.15			
FeO_{tot}	82.38	81.60	64.84	78.55	64.80	83.81
SiO_2	11.99	11.55	32.71	17.71	32.67	9.61
Total	94.37	93.15	97.70	96.26	97.47	93.42
Structural formula						
Al			0.016			
Fe^{2+}	1.445	1.434	3.004	1.637	3.006	1.361
Fe^{3+}	1.111	1.132	1.976	0.736	1.980	1.277
Si	0.445	0.434	3.004	0.637	3.006	0.362

Expt.	u693 (sk$_{100}$)	u693 (sk$_{100}$)	u702 (sk$_{100}$)	u636 (fm$_{40}$)	u636 (fm$_{40}$)	u693 (fm$_{40}$)
Phase	Gt	Sp	Gt	Gt	Sp	Sp
Al_2O_3	0.94	0.02		0.47		
FeO_{tot}	63.74	85.78	64.71	63.83	75.95	77.13
SiO_2	33.19	10.44	32.40	32.86	21.41	21.22
Total	97.87	96.24	97.29	97.16	97.36	98.35
Structural formula						
Al	0.101			0.051		
Fe^{2+}	3.031	1.381	2.996	3.029	1.756	1.743
Fe^{3+}	1.837	1.238	2.008	1.891	0.487	0.515
Si	3.031	0.381	2.996	3.029	0.756	0.743

Expt.	aw45req.	aw45req.	aw45req.	aw45 req.	u642req.	u642req.
Phase	Gt new	Gt old	Sp	Px	Gt new	Gt old
Al_2O_3	17.89	16.24	1.74	0.99	13.24	9.97
FeO_{tot}	47.02	48.23	89.60	54.61	50.94	54.25
SiO_2	35.58	35.22	2.60	43.71	34.55	34.85
Total	100.49	99.69	93.94	99.31	98.73	99.07
Structural formula						
Al	1.757	1.617	0.077	0.051	1.346	1.022
Fe^{2+}	2.965	2.975	1.098	2.032	2.980	3.031
Fe^{3+}	0.312	0.432	1.727		0.694	0.915
Si	2.965	2.975	0.098	1.945	2.980	3.031

Expt.	u642req.	u642req.	u627req.	u627req.	u627req.	aw69req.
Phase	Sp	Px	Gt old	Sp	Px	Gt rim
Al_2O_3	0.87	0.57	4.48	0.40	0.28	16.55
FeO_{tot}	86.75	54.44	60.65	85.36	54.53	47.99
SiO_2	4.93	43.51	33.38	8.39	45.38	35.74
Total	92.55	98.52	98.51	94.15	100.19	100.31
Structural formula						
Al	0.039	0.030	0.473	0.018	0.015	1.636
Fe^{2+}	1.188	20.44	2.988	1.314	1.999	2.998
Fe^{3+}	1.584		1.552	1.355		0.369
Si	0.188	1.953	2.988	0.314	1.989	2.998

TABLE 2.—*Continued*

Expt.	u835req.	u835req.
Phase	Gt new	Gt old
Al_2O_3	12.75	15.50
FeO_{tot}	51.65	49.01
SiO_2	34.77	35.24
Total	99.17	99.75
Structural formula		
Al	1.293	1.547
Fe^{2+}	2.991	2.983
Fe^{3+}	0.725	0.487
Si	2.991	2.983

0.35–0.45 mm/s, and QS = 0.29–0.75 mm/s; $^{[4]}Fe^{3+}$, IS = 0.04–0.20 mm/s, and QS = 1.05–1.28 mm/s. The hyperfine parameters of our garnet samples indicate that the Fe^{3+} is in octahedral coordination. Although the IS values are a little low compared with the range given in Amthauer et al. (1976), they are significantly larger than those observed for $^{[4]}Fe^{3+}$. Furthermore, our QS values are far too small for tetrahedral occupancy. The FWHM of this doublet is slightly larger than for the Fe^{2+} doublet, ranging mostly between 0.25 and 0.36 mm/s (Table 3). An additional very small peak occurs at ≈1.5 mm/s in the ski$_{40}$ sample (Fig. 1c). This line position is suggestive of $^{[6]}Fe^{2+}$ and could correspond to a small iron majorite ($Fe_4^{2+}Si_4O_{12}$) component in this garnet (Geiger et al., 1991). This peak was not observed in the spectrum from any other sample. At low Fe^{3+} contents, the Fe^{3+} doublet forms an ill-defined shoulder on the low-velocity Fe^{2+} peak (Fig. 1a). As a result, the Fe^{3+} line positions and calculated Fe^{3+}/Fe_{tot} are subject to relatively larger uncertainties compared with the samples richer in skiagite component. The Fe^{3+}/Fe_{tot} ratios calculated from the relative areas of the room-temperature spectra, assuming equal recoil-free fractions for Fe^{2+} and Fe^{3+} on the two sites, are in broad agreement with those calculated from the microprobe-determined compositions (Table 3). However, the Mössbauer Fe^{3+}/Fe_{tot} values systematically tend to overestimate the true value by about 15% (relative), which is probably because of our assumption of equal recoil-free fractions for Fe^{2+} and Fe^{3+}. The differences cannot be entirely reconciled by considering the uncertainties of the Mössbauer and microprobe methods, both of which are on the order of ≈0.01. The details of the Mössbauer results will be reported elsewhere.

Cell edges and molar volumes

Almandine-skiagite solutions. The garnet cell edges, a_0, are listed in Table 1 and shown in Figure 2. They increase linearly with increasing skiagite content. A weighted least-squares fit to the data gives a_0 = 11.5244(4) +

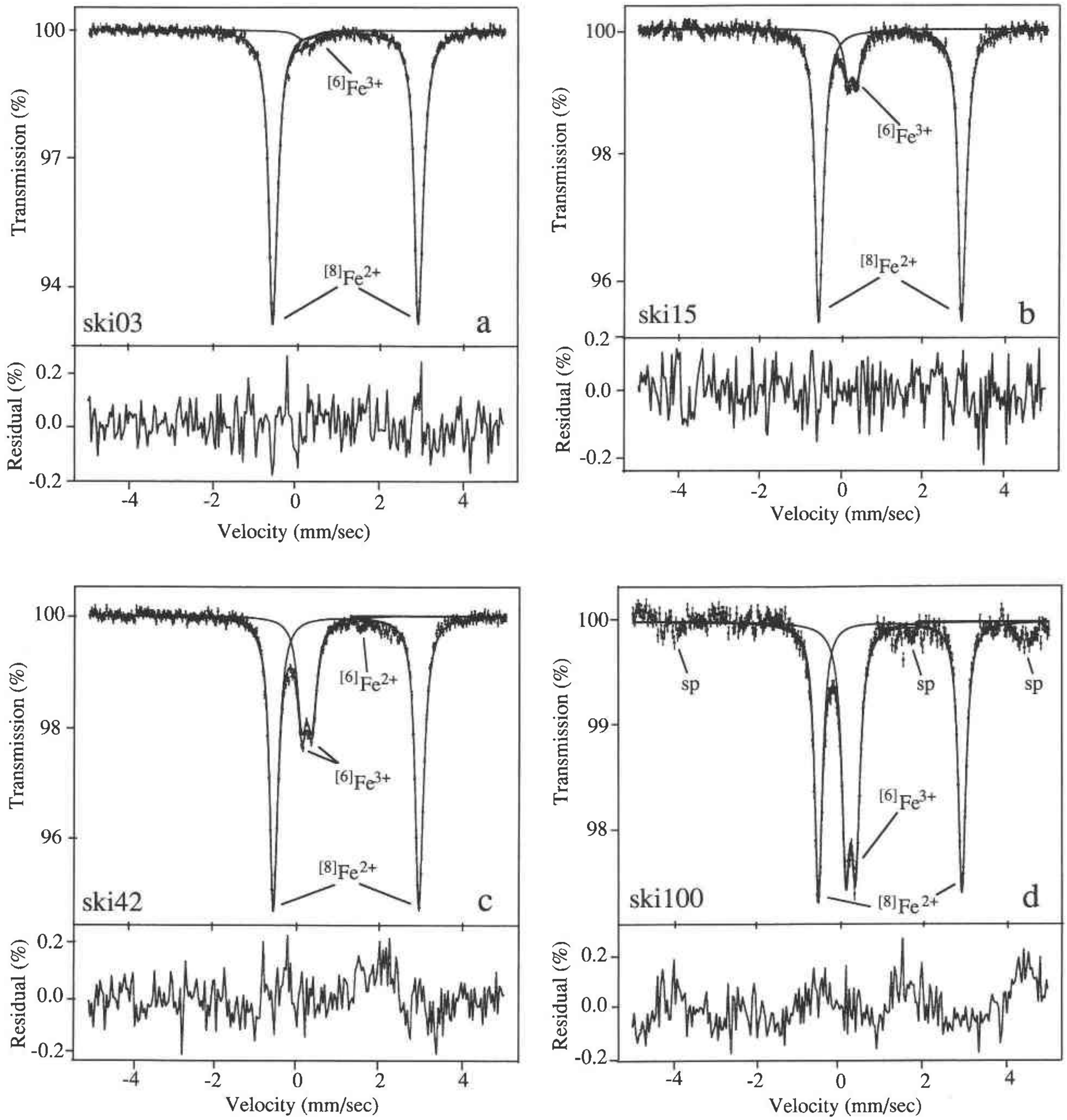

FIG. 1. Room-temperature Mössbauer spectra of four garnet samples: (**a**) ski_{03}, (**b**) ski_{15}, (**c**) ski_{42}, and (**d**) ski_{100}. The doublet with a large quadrupole splitting (QS) corresponds to Fe^{2+} in dodecahedral coordination. The doublet with a very small QS that grows with increasing skiagite content is assigned to Fe^{3+} in octahedral coordination (see text).

$0.2034(6)X_{ski}$, with $\chi^2_\nu = 1.40$. Higher order terms did not result in any significant improvement in the fit. The lattice parameters were weighted according to the standard deviations given in Table 1, and the compositions were weighted assuming estimated standard errors (of the mean) of ± 0.01 for $X_{ski} < 0.96$ and ± 0.005 for $X_{ski} > 0.96$, based upon the microprobe analyses. End-member skiagite has a cell edge of $a_0 = 11.7278(6)$ Å. Likewise, a cell edge of $a_0 = 11.5244(4)$ Å is obtained for pure almandine. This value is ~0.004 Å smaller than the the values of the almandine samples synthesized in this study; however, our almandine samples contain a small amount of Fe^{3+} (Table 3).

Skiagite. End-member skiagite was successfully synthesized from both slag and oxide mixtures. Unfortunately, variable amounts of spinel and stishovite were

Table 3. Hyperfine parameters and Fe^{3+}/Fe_{tot} ratios for almandine–skiagite garnet

Sample	Fe^{2+} QS*	Fe^{2+} IS*	FWHM (mm/s)	Fe^{3+} QS*	Fe^{3+} IS*	FWHM (mm/s)	χ^2	Fe^{3+}/Fe_{tot} area ratio
aw18(ski$_{02}$)	3.52	1.29	0.25	0.25	0.32	0.46	1.52	0.045
aw14(ski$_{03}$)	3.51	1.30	0.25	0.22	0.31	0.36	1.19	0.030
aw45(ski$_{07}$)	3.54	1.30	0.24	0.18	0.34	0.34	1.42	0.072
aw25(ski$_{08}$)	3.51	1.30	0.25	0.21	0.33	0.29	1.41	0.074
aw26(ski$_{08}$)	3.54	1.30	0.27	0.21	0.34	0.32	1.54	0.061
aw30(ski$_{09}$)	3.53	1.30	0.25	0.22	0.35	0.30	1.13	0.077
aw37(ski$_{15}$)	3.52	1.30	0.25	0.21	0.34	0.29	1.05	0.141
aw37(ski$_{21}$)	3.51	1.30	0.25	0.23	0.35	0.25	1.17	0.156
aw47(ski$_{30}$)	3.50	1.30	0.24	0.23	0.33	0.29	1.99	0.218
uhp458(ski$_{31}$)	3.51	1.29	0.28	0.23	0.35	0.28	2.04	0.191
uhp541(ski$_{42}$)	3.52	1.30	0.25	0.25	0.34	0.28	1.34	0.271
uhp627(ski$_{50}$)	3.48	1.30	0.29	0.24	0.35	0.30	1.25	0.299
uhp497(ski$_{79}$)	3.47	1.29	0.23	0.25	0.35	0.24	1.26	0.404
uhp598(ski$_{90}$)	3.50	1.30	0.24	0.24	0.36	0.25	1.24	0.429
uhp636(ski$_{100}$)	3.46	1.31	0.23	0.24	0.35	0.26	2.11	0.459
uhp702(ski$_{100}$)	3.46	1.31	0.23	0.24	0.36	0.25	1.88	0.462

Note: measurements made at 298 K and 1 atm.

* Millimeters per second measured relative to α Fe metal at 298 K. Uncertainties are about ±0.01 mm/s for both QS and IS and ±0.01 for Fe^{3+}/Fe_{tot}. The area ratio assumes the same recoil-free fraction for Fe^{2+} and Fe^{3+} on the different sites.

also present in the products. The best yield of garnet (on the order of 60–70%) was obtained from stoichiometric mixtures of ferrosilite + hematite. The minimum pressure at which the end-member skiagite is stable is about 9.3 GPa, based upon the observed growth of garnet on garnet seeds in backscattered electron images from experiment uhp666.

The molar volume (V_{298}) for the skiagite end-member is 121.44 cm³. Karpinskaya et al. (1982) were the first to report the synthesis of skiagite. They produced a mixture of garnet, spinel, and stishovite? at 800 °C and 10.0 GPa and reported a molar volume of 120.9 ± 1.5 cm³ for the garnet. The large uncertainty in their measurement is attributable to their analytical method (Gandolfi camera) and the presence of spinel, which has many overlapping reflections with the garnet. The molar volume of skiagite determined in this study is in good agreement with that predicted from crystal structure considerations by Novak and Gibbs (1971), 121.2 cm³.

Almandine. The molar volume of pure $Fe^{2+}_3Al_2Si_3O_{12}$ determined from extrapolation of our binary garnet data, 115.23 ± 0.01 cm³, falls within the range of values reported in the literature: 115.28 cm³ from Cressey et al. (1978) and Geiger et al. (1987), 115.20–115.34 cm³ from Bohlen et al. (1983b), 115.25–115.43 cm³ from Hsu (1968), and 115.19–115.40 cm³ from Keesman et al. (1971). Our garnet sample with the smallest molar volume, 115.34 cm³, was synthesized in the presence of excess SiO_2 and Fe metal, yet it contained detectable Fe^{3+} (aw1, aw6; Table 1). This confirms that small quantities of Fe^{3+} are readily accommodated in almandine at very low f_{O_2}, even in the presence of Fe metal. The coexistence of Fe^{3+}-bearing almandine and Fe metal suggests that macroscopically stoichiometric almandine may not be stable, at least at the conditions of the syntheses.

The range in molar volumes cited above, although small, is significantly greater than the accuracy and precision of the measurement of the unit-cell edge by X-ray diffraction. This points to small differences in composition, possibly even involving defects, among the various synthesized almandine samples. Some of the almandine samples reported by Hsu (1968) were synthesized hydrothermally and could well contain H_4O_4 groups that would increase the garnet unit-cell edge (e.g., Meagher, 1980). Our results document that the incorporation of a skiagite component also increases the unit-cell edge. With the experimental difficulty in maintaining all Fe in the Fe^{2+} state, many of the reported values larger than our extrapolated value probably reflect the presence of variable amounts of Fe^{3+}. This has sometimes led to the assump-

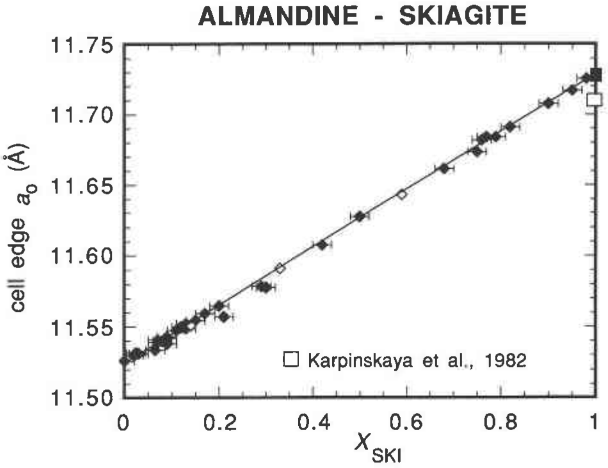

Fig. 2. Cell edge, a_0, vs. composition for almandine-skiagite solutions. The linear regression shown is based upon the solid data points only. The solid diamonds are data from this study. The solid square at the skiagite end-member is in perfect agreement with the extrapolated value from this regression. The open diamonds indicate the garnet composition attending reequilibration at lower pressure. The open square is from Karpinskaya et al. (1982), which is the only other report of a synthesis of skiagite.

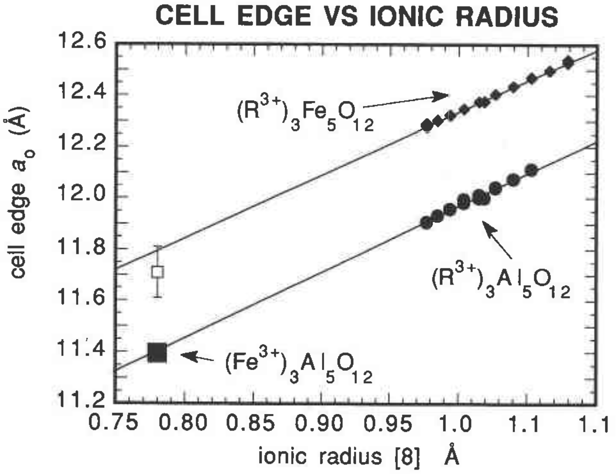

Fig. 3. Unit-cell edge vs. the dodecahedral cation ionic radius for rare-earth garnets with $R_3^{3+}Fe_5O_{12}$ and $R_3^{3+}Al_5O_{12}$ stoichiometry. The ionic radii are from Shannon (1976). The cell edge data are from Rubinstein and Barns (1964), JCPDS X-ray diffraction cards 22-1093, 32-12, 32-16, and the compilations of Hawthorne (1981) and Stadnik (1984). The open square is for the end-member Fe_8O_{12} (garnet), based on extrapolation from $(Y,Fe^{3+})_3Fe_5^{3+}O_{12}$ garnet solution, with the error bar assuming an uncertainty in composition of ±10% (relative) (Paladino and Maguire, 1970). The solid square shows the position of the hypothetical $Fe_3^{3+}Al_5O_{12}$ (garnet) obtained by extrapolation.

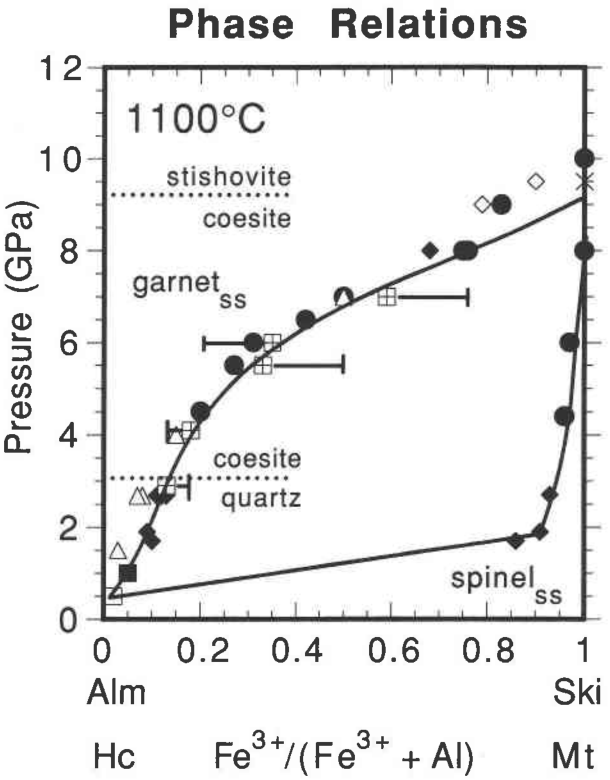

Fig. 4. Phase relations for almandine-skiagite solutions as a function of pressure up to 12.0 GPa at 1100 °C. The coexisting spinel composition, defining part of the loop, is shown projected through Fe_2SiO_4, which makes the loop pseudodivariant. The positions of the SiO_2 polymorph transitions are also shown for reference. Open triangles are garnet ± SiO_2; open diamonds are garnet + hematite + SiO_2; closed diamonds are garnet + spinel + SiO_2 + pyroxene; closed circles are garnet + spinel + SiO_2; crossed squares are the reequilibration experiments with the approach to equilibrium shown; the × indicates no reaction; the closed square is garnet + fayalite + spinel + quartz; the open square is the terminal reaction almandine = hercynite + fayalite + quartz, calculated from the thermodynamic data base of Holland and Powell (1990).

tion that the lower the unit-cell edge, the lower the Fe^{3+} content, and therefore the closer to the ideal stoichiometric almandine. However, Bohlen et al. (1983b) synthesized almandine garnet with cell edges of 11.520 and 11.521 Å, considerably smaller than our extrapolated value. Minor substitution of another type of component would appear to be a likely explanation. One such possibility is an Fe^{3+}-bearing component analogous to YAG, $Fe_3^{3+}Al_5O_{12}$. In almandine, this would be achieved through the coupled substitution of Fe^{3+} for Fe^{2+} and Al for Si on the dodecahedral and tetrahedral sites, respectively. Yoder and Keith (1951) demonstrated a complete solid solution between $Mn_3Al_2Si_3O_{12}$ and $Y_3Al_5O_{12}$, suggesting that there is no difficulty in substituting Al for Si on the tetrahedral sites of silicate garnets. A small amount of $^{[8]}Fe^{3+}$ may be inferred to occur in $Y_3Fe_5O_{12}$ garnet in equilibrium with Fe_2O_3 at high temperatures (Paladino and Maguire, 1970). At 1450 °C and 1 atm, Paladino and Maguire (1970) showed an excess of Fe_2O_3 in the garnet, equivalent to 0.9 mol% Fe_8O_{12}, which caused a decrease in a_0 of 0.006 Å. In Figure 3, we have plotted the unit-cell edge vs. dodecahedral cation ionic radius for rare-earth $R_3^{3+}Al_5O_{12}$ and $R_3^{3+}Fe_5O_{12}$ garnets. Both the ferrite garnet and aluminate garnet define linear relationships with nearly identical slopes, emphasizing the strong influence the dodecahedral cation plays in determining the molar volume of these garnets. A linear extrapolation to 0.78 Å (Fe^{3+} in eightfold coordination) yields a_0 = 11.39 Å, or V = 111.0 cm³, for the hypothetical $Fe_3^{3+}Al_5O_{12}$ component. The unit-cell edge reported by Bohlen et al. (1983b) would correspond to about 2 mol% of this component, consistent with the Fe^{3+}/Fe_{tot} of 0.02 ± 0.01 measured by Mössbauer spectroscopy of their sample. This substitution would be favored by an SiO_2-poor composition and high Al_2O_3 activity. It is therefore possible that minor amounts of solid solution can act to reduce the unit-cell edge of almandine as well as increase it, and the assumption that the lowest cell edge corresponds to the most stoichiometric composition is not necessarily valid. The unit-cell edge from the regression of our data should provide the best estimate for pure stoichiometric almandine.

Phase relations

The extent of Fe^{3+} substitution for Al in garnet increases strongly with increasing pressure (Table 1). The results can be conveniently viewed in terms of an isothermal quasi-divariant system projected from a point along the Fe_2SiO_4-SiO_2 join onto the Al-Fe^{3+} pressure plane. This is illustrated in Figure 4, which shows the phase relations with the garnet solutions as a function of pressure. For example, at 1100 °C, the skiagite component saturates at 13, 43, and 75 mol% at 2.7, 6.5, and 8.0 GPa, respectively. The skiagite end-member is stable above ≈9.3 GPa. When the starting material has an Fe^{3+}/Fe_{tot} content that differs from the stable garnet composition at a particular pressure, a multiphase assemblage appears. The coexisting phases and their compositions obviously depend on the starting bulk composition. However, here we are concerned with compositions that lie on or very close to the almandine-skiagite join.

Under dry conditions and low pressures, the stability field of garnet terminates with the equilibrium

$$\underset{\text{garnet}}{Fe_3Al_2Si_3O_{12}} = \underset{\text{spinel}}{FeAl_2O_4} + \underset{\text{fayalite}}{Fe_2SiO_4} + \underset{\text{quartz}}{2SiO_2}$$

$$\Delta V^{\circ}_{1,298} = 21.03\ \text{cm}^3 \qquad (1a)$$

or

$$\underset{\text{garnet}}{Fe^{2+}_3Fe^{3+}_2Si_3O_{12}} = \underset{\text{spinel}}{Fe_3O_4} + \underset{\text{fayalite}}{Fe_2SiO_4} + \underset{\text{quartz}}{2SiO_2}$$

$$\Delta V^{\circ}_{1,298} = 14.75\ \text{cm}^3 \qquad (1b)$$

(Keesman et al., 1971; Hensen, 1970). Molar volumes are from this study and Holland and Powell (1990). Reaction 1a, the essentially Fe^{3+}-free reaction, lies at about 0.5 GPa at 1100 °C (Hensen, 1970). At higher pressure, fayalite + quartz becomes unstable relative to orthopyroxene, and the garnet composition is governed by the equilibrium

$$\underset{\text{garnet}}{Fe_3Al_2Si_3O_{12}} = \underset{\text{spinel}}{FeAl_2O_4} + \underset{\text{orthopyroxene}}{Fe_2Si_2O_6} + \underset{\text{quartz/coesite}}{SiO_2}$$

$$\Delta V^{\circ}_{1,298} = 14.16\ \text{cm}^3 \qquad (2a)$$

or

$$\underset{\text{garnet}}{Fe^{2+}_3Fe^{3+}_2Si_3O_{12}} = \underset{\text{spinel}}{Fe_3O_4} + \underset{\text{orthopyroxene}}{Fe_2Si_2O_6} + \underset{\text{quartz/coesite}}{SiO_2}$$

$$\Delta V^{\circ}_{1,298} = 11.73\ \text{cm}^3 \qquad (2b)$$

The $\Delta V^{\circ}_{1,298}$ given is with coesite. This phase assemblage is shown at a representative pressure of 2.7 GPa in Figure 5, plotted in the composition space FeO-SiO_2-($AlO_{1.5}$ + $FeO_{1.5}$). The coexisting orthopyroxene contains only minor amounts of Al, ≤0.09 cations on a six O atom basis for all experiments. The coexisting spinel is an Fe_3O_4-Fe_2SiO_4-$FeAl_2O_4$ solution in which the $FeAl_2O_4$ component decreases sharply with increasing pressure (Table 1, Fig. 4). For example, the spinel in equilibrium with garnet (ski_{13}) at 2.7 GPa has a composition of 87% Fe_3O_4 + 8% Fe_2SiO_4 + 5% $FeAl_2O_4$. With increasing pressure there is a progressive increase in the solubility of Fe_2SiO_4 in the spinel, such that orthopyroxene + Si-poor spinel becomes unstable relative to Si-rich spinel + SiO_2. This results in the following high-pressure equilibrium with garnet (Fig. 5):

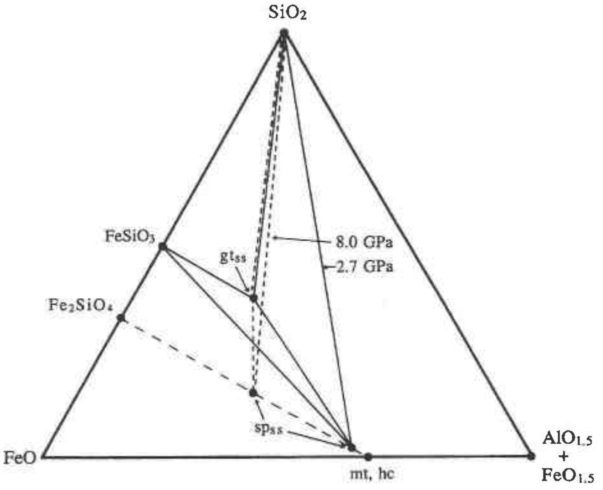

Fig. 5. Plot of the system FeO-SiO_2-($AlO_{1.5}$ + $FeO_{1.5}$) showing representative phase assemblages at 2.7 and 8.0 GPa and 1100 °C. Note the shift in spinel composition with increasing pressure.

$$\underset{\text{garnet}}{Fe_3Al_2Si_3O_{12}} = \underset{\text{spinel}}{FeAl_2O_4} + \underset{\text{spinel}}{Fe_2SiO_4} + \underset{\text{coesite/stishovite}}{2SiO_2}$$

$$\Delta V^{\circ}_{1,298} = 8.60\ \text{cm}^3\ \text{(for coesite)} \qquad (3a)$$

or

$$\underset{\text{garnet}}{Fe^{2+}_3Fe^{3+}_2Si_3O_{12}} = \underset{\text{spinel}}{Fe_3O_4} + \underset{\text{spinel}}{Fe_2SiO_4} + \underset{\text{coesite/stishovite}}{2SiO_2}$$

$$\Delta V^{\circ}_{1,298} = 6.17\ \text{cm}^3\ \text{(for coesite).} \qquad (3b)$$

The $\Delta V^{\circ}_{1,298}$ of γ Fe_2SiO_4 (spinel), 41.77 cm³, is extrapolated from the Al-free spinels in Table 1 and from Canil and O'Neill (unpublished data). At high pressure, the spinel contains even less Al. For example, the spinel in equilibrium with garnet (ski_{82}) is essentially 55% Fe_3O_4 + 45% Fe_2SiO_4 with <1.0 mol% $FeAl_2O_4$ (Table 1). Note that the spinel compositions in Figure 4 have been projected through Fe_2SiO_4 to plot them on the diagram. Thus, the loop shown is quasi-divariant and could cause the false impression that the spinel coexisting with skiagite-rich garnets is virtually pure magnetite, when in fact they contain appreciable Fe_2SiO_4. The increase in Fe_2SiO_4 content of the spinel with increasing pressure is evident when comparing the compositions of the spinels in the phase assemblages at 2.7 and 8.0 GPa in the projection of Figure 5.

In several experiments, the starting Fe^{3+}/Fe_{tot} clearly deviated from the stable garnet composition, causing phases other than those involved in Reactions 2 and 3 to appear. When the starting composition was too oxidized (excess Fe^{3+}), such as in experiment uhp497, hematite appeared instead of spinel (Table 1). When the starting composition was too reduced (excess Fe^{2+}), an SiO_2 deficient assemblage was produced. At high pressure, py-

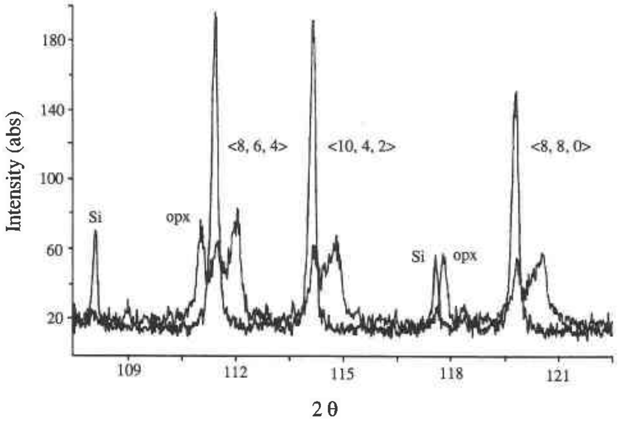

Fig. 6. High-angle ⟨8,6,4⟩, ⟨10,4,2⟩, and ⟨8,8,0⟩ reflections from a reequilibrated garnet (short peaks) and its ski$_{78}$ precursor (monochromated Co$K\alpha_1$ radiation).

roxene appeared at the expense of coesite [uhp532 (ski$_{70}$)]. It was identified as clinoferrosilite, on the basis of several low-intensity peaks on the X-ray diffraction pattern. The occurrence of clinoferrosilite rather than orthoferrosilite at 8.0 GPa and 1100 °C is consistent with the results of Akimoto et al. (1965). In a lower pressure experiment, aw26, fayalite was produced at the expense of quartz.

Reversals. Three experiments were performed where a previously synthesized garnet was reequilibrated at lower pressure. A new garnet, richer in almandine content, formed (Figs. 2, 4, 6). In these experiments, therefore, equilibrium was approached from the direction of relatively high Fe^{3+} in the garnet. Two distinct peaks at high 2θ are observable in the powder diffractograms from these experiments, an example of which is presented in Figure 6. One peak corresponds to the original garnet, which has not fully reacted, and the other peak corresponds to the newly crystallized garnet. Only the cell edge of the new garnet is reported in Table 1. The presence of two distinct peaks rather than a single broad peak shows that the new garnet formed by the breakdown of the original garnet followed by nucleation and growth rather than by coupled diffusion of Al and Fe^{3+}. This is confirmed by the textures observed in backscattered electron images.

The approach to equilibrium from the direction of relatively high Al content in the garnet was tested in two experiments (aw69, uhp835; see Table 1). In aw69, a previously synthesized assemblage of garnet (ski$_{13}$) + spinel + pyroxene + quartz was reacted at a higher pressure of 4.1 GPa. The resulting large garnets (>10 μm) were zoned, and small grains (3–8 μm) showed a range in composition. The most skiagite-rich composition (ski$_{18}$) was taken as that most closely representing the maximum skiagite solubility at the higher pressure, and it is given in Tables 1 and 2. In the other experiment (uhp835) a mixture of ferrosilite, hematite, and a previously synthesized garnet (ski$_{21}$) were reacted at 6.0 GPa. Skiagite-rich rims were observed to have grown on the original garnet grains. The rim compositions were variable, presumably because of a heterogenous distribution of hematite at the required fine scale in the starting mixture. The most skiagite-rich rim was taken to be closest to the equilibrium composition (Tables 1, 2). The difficulty in obtaining homogeneous garnet in these experiments is analogous to the difficulty in synthesizing garnet solid solutions from oxide mixes, as described earlier. In contrast, the garnets produced from glass or slag were not zoned. The lack of zoning under *P-T* conditions where nonequilibrium garnets show zoning suggests that the use of glasses or slags produced equilibrium garnet compositions.

Skiagite solubility in almandine has a strong positive pressure dependence (Fig. 4). A sharp increase in skiagite solubility occurs at pressures above ≈5.0 GPa. The change in slope illustrated in Figure 4 is attributable to the disappearance of pyroxene as a coexisting phase and represents the transition from breakdown Reactions 3 to 4. The strong pressure dependence in skiagite solubility can be understood in part by considering the $\Delta V^\circ_{1,298}$ for the skiagite breakdown Reaction 3b. With coesite as the SiO$_2$ polymorph, $\Delta V^\circ_{1,298} = +6.17$ cm^3. Therefore, skiagite is expected to be favored with increasing pressure. Such an argument does not hold in the stishovite stability field, however, where Reaction 3b gives $\Delta V^\circ_{1,298} = -7.5$ cm^3. Skiagite should be destabilized by the transformation from coesite to stishovite. This is consistent with the absence of garnet in a reconnaissance experiment using a stoichiometric mixture of ferrosilite and hematite performed at 13.0 GPa and 1100 °C. It appears that at 1100 °C, end-member skiagite is only stable within a narrow pressure range just above the coesite-stishovite transition.

The Al content of the coexisting spinel varies widely depending on the amount of skiagite in the garnet. At low pressures, nearly pure hercynite coexists with almandine (Reaction 1a, 1b; Fig. 4). The incorporation of a small skiagite component in the garnet drives the spinel to magnetite-rich compositions (Fig. 4). Except at dilute skiagite compositions (<10 mol% skiagite), hercynite is only a minor component in the spinel. This indicates that Al is strongly partitioned into garnet.

An iron majorite component?

Majorite, (Mg,Fe^{2+})$_4$Si$_4$O$_{12}$, is believed to be an abundant garnet component at depths >350 km (Ringwood, 1975). According to Akaogi and Akimoto (1977), the solubility of iron majorite in almandine reaches a maximum of 40 mol% between 9.0 and 10.0 GPa at 1000 °C. They estimated a unit-cell edge of 11.595 Å for the Fe$^{2+}_4$Si$_4$O$_{12}$ end-member, based on extrapolation. However, the solubility of an iron majorite component in Fe^{3+}-bearing garnet has not been previously studied. No significant excess of Si (>3.0 cations pfu) was detected by the electron microprobe. A trace of $^{[6]}$Fe^{2+} was detected in only one Mössbauer spectrum, sample uhp541, with a composition of 40% skiagite + 60% almandine (Fig. 1c). This suggests that at least small amounts of iron majorite can be accommodated in the presence of Fe^{3+}. Confident identification of $^{[6]}$Fe^{2+} in the end-member samples is hampered by the presence of small amounts of spinel, which have overlapping peak positions with any $^{[6]}$Fe^{2+} in the garnet (compare Fig. 1c and 1d). Two experiments were performed in the FeO-FeO$_{1.5}$-SiO$_2$ subsystem with a bulk composition of 60% skiagite and 40% iron majorite to test for the possible solubility of iron majorite in skiagite [uhp636 (ski$_{60}$-fm$_{40}$) and uhp693 (ski$_{60}$-fm$_{40}$)]. Garnets with cell edges slightly smaller than that for the pure skiagite end-member were produced in both experiments (Table 1). However, a small amount of Al was detected in the garnets by microprobe, indicating some contamination had occurred, probably during loading of the capsule. The smaller cell edges are in good agreement with the determined almandine content in these samples. These experiments suggest that the solubility of iron majorite in skiagite is very small; otherwise the measured cell edges would have deviated significantly from the pure end-member value. The garnet in equilibrium with these Fe$_2$SiO$_4$-rich spinels + SiO$_2$ should have the greatest possible majorite content, yet little if any is indicated. However, that does not preclude significant solubility of Fe^{3+} in majorite-rich garnet at higher pressures. In fact, a recent synthesis of (Mg$_{0.8}$Fe$_{0.2}$)SiO$_3$ garnet at 1800 °C and 18 GPa was found to have up to 14% of its Fe in the ferric state, corresponding to 5 mol% of an Fe$_3^{2+}$Fe$_2^{3+}$-Si$_3$O$_{12}$, or skiagite, component (O'Neill et al., 1993).

Free energy of formation of $Fe_3^{2+}Fe_2^{3+}Si_3O_{12}$ at 1100 °C

An estimate of $\Delta_f G^\circ_{1,1373}$ for skiagite can be made from the experiments in Table 1 by considering the exchange reaction

$$\underset{\text{garnet}}{\tfrac{1}{2}\mathrm{Fe_3^{2+}Fe_2^{3+}Si_3O_{12}}} + \underset{\text{spinel}}{\tfrac{1}{2}\mathrm{FeAl_2O_4}}$$

$$= \underset{\text{garnet}}{\tfrac{1}{2}\mathrm{Fe_3Al_2Si_3O_{12}}} + \underset{\text{spinel}}{\tfrac{1}{2}\mathrm{Fe_3O_4}} \quad \Delta V^\circ_{1,298} = -1.22\ \mathrm{cm^3} \quad (4)$$

for which

$$\Delta G^\circ_{P,1373} = -\tfrac{1}{2}RT \ln \frac{a^{\mathrm{sp}}_{\mathrm{Fe_3O_4}} a^{\mathrm{gt}}_{\mathrm{Fe_3Al_2Si_3O_{12}}}}{a^{\mathrm{sp}}_{\mathrm{FeAl_2O_4}} a^{\mathrm{gt}}_{\mathrm{Fe_3Fe_2Si_3O_{12}}}}$$

$$= -RT \ln K_d - RT \ln K_\gamma$$

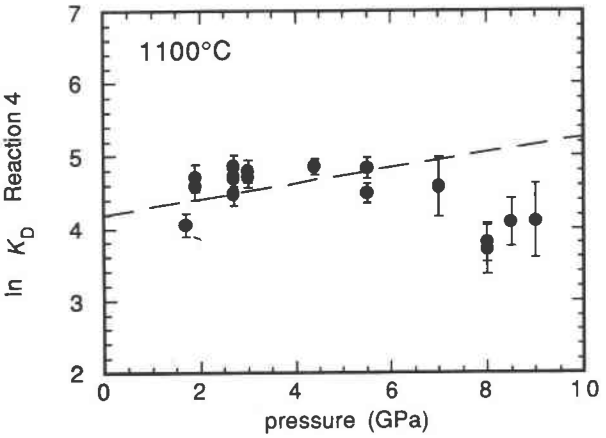

Fig. 7. Plot of ln K_d vs. pressure for Reaction 4. The uncertainties are 1σ, computed from the microprobe analyses of the garnet and spinel. The slope of the line shown was constrained by d(ln K)/dP = $-\Delta V^\circ_{1,298}/RT$; however, the actual position is from a best fit by eye. The slope of 1.069 × 10^{-5}/bar assumes ideal mixing behavior (i.e., $K = K_d$).

where $a = (X\gamma)^2$ for both spinel and garnet. The standard state is the pure substance at 1 bar and the temperature of interest. Figure 7 is a plot of ln K_d as a function of pressure. With $\int_1^P \Delta V_{P\text{-}T}\, \mathrm{d}P = \Delta V_{1,298}\Delta P$ and both the garnet and spinel as ideal solid solutions, ln K_d should be a linear function of pressure with slope d(ln K_d)/dP = d(ln K)/dP = $-\Delta V^\circ_{1,298}/RT$. A line with this slope (1.069 × 10^{-5}/bar) is drawn in Figure 7, with the actual position fitted by eye. The lack of agreement with the data indicates that one or both of the phases are nonideal. Nonideality in the ternary Fe$_3$O$_4$-FeAl$_2$O$_4$-Fe$_2$SiO$_4$ spinels is plausible. However, nothing is presently known about the thermodynamic mixing properties of 2-3 spinels, such as Fe$_3$O$_4$ and FeAl$_2$O$_4$, with 4-2 silicate spinels (O'Neill and Navrotsky, 1984). Restricting our analysis to those data below 4.5 GPa, where $X_{\mathrm{Fe_2SiO_4}}$ are sufficiently small, we can reasonably project our spinel compositions from Fe$_2$SiO$_4$ onto the Fe$_3$O$_4$-FeAl$_2$O$_4$ binary and calculate $\gamma_{\mathrm{FeAl_2O_4}}$ and $\gamma_{\mathrm{Fe_3O_4}}$, following the model of O'Neill and Navrotsky (1984). If we assume ideal mixing in the coexisting garnet, the $\gamma_{\mathrm{ski}}/\gamma_{\mathrm{alm}}$ term will drop out of the equation. Alternatively, Luth et al. (1990) provide an estimate for the Al-Fe^{3+} mixing properties in garnets of $W_{\mathrm{Al\text{-}Fe^{3+}}} = 3.7$ kJ/mol on a per cation basis. Treating the spinel solid solutions in the above manner and assuming $\int_1^P \Delta V_{P\text{-}T}\, \mathrm{d}P = \Delta V_{1,298}\Delta P$ we can express $\Delta G^\circ_{1,1373}$ for the exchange Reaction 4 as:

$$\Delta G^\circ_{1,1373} = -RT \ln K_d - RT \ln \frac{\gamma_{\mathrm{Fe_3O_4}}}{\gamma_{\mathrm{FeAl_2O_4}}}$$

$$- P\Delta V^\circ_{1,298}\ (\text{Reaction 4}) + RT \ln \frac{\gamma_{\mathrm{ski}}}{\gamma_{\mathrm{alm}}}.$$

From the ten data below 4.5 GPa, we obtain $\Delta G^\circ_{1,1373} = -34.63$ kJ/mol, with a σ of 1.51 kJ if mixing in the garnet is ideal, and $\Delta G^\circ_{1,1373} = -31.83 \pm 1.57$ kJ/mol if the interaction parameter of Luth et al. (1990) is considered. Taking the free energies of formation for almandine, magnetite, and hercynite at 1373 K derived from Holland and Powell (1990) and using entropies of Si and O$_2$ from Robie et al. (1978) and of Fe from Holmes et al. (1986) gives for skiagite $\Delta_f G^\circ_{1,1373}$ (ski) = -2975.2 ± 3.0 kJ/mol for the case of ideal almandine-skiagite mixing and $\Delta_f G^\circ_{1,1373}$ (ski) = -2980.8 ± 3.1 kJ/mol with the symmetric interaction parameter, $W_{\mathrm{Al\text{-}Fe^{3+}}}$, of Luth et al. (1990). The data of Holmes et al. (1986) were used for Fe because Holland and Powell (1990) only tabulate data for α Fe, and our calculations, at 1373 K, are in the γ Fe field. The quoted uncertainties do not include any contribution derived from uncertainties in the thermodynamic data for the other phases.

With the above result and Holland and Powell's data for grossular, almandine, and andradite combined, the ΔG for the reciprocal reaction,

$$\underset{\text{almandine}}{Fe_3^{2+}Al_2Si_3O_{12}} + \underset{\text{andradite}}{Ca_3Fe_2^{3+}Si_3O_{12}} = \underset{\text{skiagite}}{Fe_3^{2+}Fe_2^{3+}Si_3O_{12}} + \underset{\text{grossular}}{Ca_3Al_2Si_3O_{12}} \qquad (5)$$

is estimated to be $\Delta G^\circ_{P,1373}$(kJ/mol) = 40.2 − 0.7P (GPa) from Reaction 5 with ideal mixing, and $\Delta G^\circ_{P,1373}$ (kJ/mol) = 32.8 − 0.7P using the interaction parameter of Luth et al. for Al-Fe^{3+} mixing. The relatively large value of $\Delta G^\circ_{P,1373}$ (Reaction 5) is presumably due to the fact that the octahedral cation to O bond distances in garnet (i.e., Al-O and Fe^{3+}-O) are a strong function of the dodecahedral cation size and vice versa: the $^{[8]}$Ca-O and Fe^{2+}-O bond distances depend on the size of the octahedral cation. If that is true, then the analogous reciprocal reaction involving the magnesium garnets, pyrope and khoharite ($Mg_3Fe_2^{3+}Si_3O_{12}$), would be expected to have a similar ΔG as the Fe-bearing Reaction 5 because of the similarity in ionic radii of Mg and Fe^{2+} in dodecahedral coordination (Shannon, 1976).

The value of ΔG for the reciprocal Reaction 5 is intermediate between the two values, 25 and 50 kJ/mol, assumed by Luth et al. (1990). When applied to their equilibria used to calculate mantle f_{O_2}, resulting f_{O_2} values generally fall within the range of FMQ ± 1.5 log units (Luth et al., 1990, their Fig. 7a–7c). This implies redox conditions in the garnet lherzolite facies of the upper mantle similar to those observed in the spinel lherzolite facies (Wood et al., 1990).

The question of whether pure almandine is stable in light of our experiments with excess Fe metal and quartz can be assessed by considering the reaction

$$\underset{\text{garnet}}{\tfrac{1}{3}Fe_3^{2+}Fe_2^{3+}Si_3O_{12}} = \underset{\text{metal}}{\tfrac{5}{3}Fe} + \underset{\text{quartz}}{SiO_2} + O_2$$

$$\Delta V^\circ_{1,298} = -4.99\ \text{cm}^3. \qquad (6)$$

If the Fe and quartz are pure (a = 1.0), $\log K_6 = \log f_{O_2} - \tfrac{1}{3}\log a_{ski}$. With data for β quartz from Holland and Powell (1990) for O_2 and Fe from Robie et al. (1978) and Holmes et al. (1986), $\log K_6 = -12.06$ at 1373 K and 2.0 GPa, assuming ideal mixing in the garnet. With a log f_{O_2} defined by the O_2 buffer assemblage quartz + fayalite + Fe (QFI), extrapolated to 1373 K and 2.0 GPa ($\log f_{O_2} = -13.29$; O'Neill, 1987), this yields $\log a_{ski} = -3.69$ or X_{ski} = 1.4 mol%. The QFI buffer lies close to the low f_{O_2} stability limit for almandine (Woodland and Wood, 1989), and, therefore, the skiagite content under these conditions should be near the minimum possible. The calculated skiagite content is in close agreement with that indicated from the unit-cell edge measurements of our experiments with excess Fe and SiO_2 performed at higher temperature (X_{ski} = 2 mol% in aw1, aw6; Table 1). The sign of $\Delta V^\circ_{1,298}$ (Reaction 6) shows that slightly lesser skiagite contents would be favored at lower pressure. The influence of temperature is not known.

CONCLUSIONS

Fe^{3+} is readily accommodated in the aluminous garnet almandine. Substitution of Fe^{3+} for Al on the octahedral sites can be considered in terms of an $Fe_3^{2+}Fe_2^{3+}Si_3O_{12}$ (skiagite) component. The maximum extent of skiagite solubility in almandine is strongly pressure dependent, increasing with increasing pressure. At high pressure, the solid solution is complete. End-member skiagite is stable at pressures above ≈9.3 GPa. The molar volume of skiagite, 121.45 ± 0.01 cm³, agrees with the value reported by Karpinskaya et al. (1982), although our value is both more accurate and more precise. Molar volumes of the almandine-skiagite solid solutions vary linearly with composition. The molar volume of almandine retrieved from the fit to our data is 115.23 ± 0.01 cm³. Small differences from this value reported by other workers may be due to minor amounts of other components.

The maximum solubility of Fe^{3+}, or the skiagite component, in garnet at a given pressure is controlled through the equilibrium between garnet and the assemblage spinel + SiO_2 + orthopyroxene at low pressures (<5.0 GPa) or spinel + SiO_2 at high pressure. The coexisting spinel becomes progressively richer in Fe_2SiO_4, with increasing pressure to the point where the Fe^{3+}/Fe_{tot} of the spinel approaches that of the garnet. The very low Al content of both the coexisting spinel and pyroxene indicates that Al is strongly partitioned into garnet.

End-member skiagite probably becomes unstable with increasing pressure in the stishovite stability field. As a result, this garnet is only stable within a rather narrow pressure range, at least at 1100 °C. Iron majorite substitution in skiagite is negligible at the pressures of this study. The demonstrated ability of a pyralspite garnet sample to contain substantial Fe^{3+} suggests that garnet could be the dominant Fe^{3+}-bearing phase in the mantle at pressures above the stability limit of aluminate-chromite spinel.

ACKNOWLEDGMENTS

This project was made possible in part by a fellowship to A.B.W. from the Alexander von Humboldt Stiftung. Its support is gratefully acknowledged. D. Canil, V. von Seckendorf, C. McCammon, and F. Seifert are thanked for their helpful advice and discussion during the course of the project. The manuscript was improved through the thoughtful reviews of C. Manning, W. Dollase, D. Perkins, and an anonymous reviewer.

REFERENCES CITED

Akaogi, M., and Akimoto, S. (1977) Pyroxene-garnet solid solution equilibria in the systems $Mg_4Si_4O_{12}$-$Mg_3Al_2Si_3O_{12}$ and $Fe_4Si_4O_{12}$-$Fe_3Al_2Si_3O_{12}$ at high pressures and temperatures. Physics of the Earth and Planetary Interiors, 15, 90–106.

Akimoto, S., Katsura, T., Syono, Y., Fujisawa, H., and Komado, E. (1965) Polymorphic transition of $FeSiO_3$ and $CoSiO_3$ at high pressures and temperatures. Journal of Geophysical Research, 70, 5269–5278.

Amthauer, G., Annersten, H., and Hafner, S.S. (1976) The Mössbauer spectrum of ^{57}Fe in silicate garnets. Zeitschrift für Kristallographie, 143, 14–55.

Bohlen, S.R., and Boettcher, A.L. (1982) The quartz = coesite transformation: A precise determination and the effects of other components. Journal of Geophysical Research, 87, 7073–7078.

Bohlen, S.R., Essene, E.J., and Boettcher, A.L. (1980) Reinvestigation and application of olivine-quartz-orthopyroxene barometry. Earth and Planetary Science Letters, 47, 1–10.

Bohlen, S.R., Dollase, W.D., and Wall, V.J. (1983a) Calibration and applications of spinel equilibria in the system FeO-Al_2O_3-SiO_2. Journal of Petrology, 27, 1143–1156.

Bohlen, S.R., Wall, V.J., and Boettcher, A.L. (1983b) Experimental investigations and geological applications of equilibria in the system FeO-TiO_2-Al_2O_3-SiO_2-H_2O. American Mineralogist, 68, 1049–1058.

Cressey, G., Schmid, R., and Wood, B.J. (1978) Thermodynamic properties of almandine-grossular garnet solid solutions. Contributions to Mineralogy and Petrology, 67, 397–404.

Geiger, C.A., Newton, R.C., and Kleppa, O.J. (1987) Enthalpy of mixing of synthetic almandine-grossular and almandine-pyrope garnets from high temperature solution calorimetry. Geochimica et Cosmochimica Acta, 51, 1755–1763.

Geiger, C.A., Rubie, D.C., Ross, C.R., II, and Seifert, F. (1991) A cation partitioning study of (Mg,Fe)SiO_3 garnet using ^{57}Fe Mössbauer spectroscopy. Eos, 72, 564–565.

Hackler, R.T., and Wood, B.J. (1989) Experimental determination of Fe and Mg exchange between garnet and olivine and estimation of Fe-Mg mixing properties in garnet. American Mineralogist, 74, 994–999.

Hawthorne, F.C. (1981) Some systematics of the garnet structure. Journal of Solid State Chemistry, 37, 157–164.

Hensen, B.J. (1970) Experimental determination of the stability of cordierite and garnet in pelitic compositions and high pressures and temperatures. Ph.D. thesis, Australian National University, Canberra.

Holland, T.J.B. (1980) The reaction albite = jadite + quartz determined experimentally in the range 600–1200 °C. American Mineralogist, 65, 129–134.

Holland, T.J.B., and Powell, R. (1990) An enlarged and updated internally consistent thermodynamic dataset with uncertainties and correlations: The system K_2O-Na_2O-CaO-MgO-MnO-FeO-Fe_2O_3-Al_2O_3-TiO_2-SiO_2-C-H_2-O_2. Journal of Metamorphic Petrology, 8, 89–124.

Holmes, R.D., O'Neill, H.St.C., and Arculus, R.J. (1986) Standard Gibbs free energy of formation for Cu_2O, NiO, CoO, and Fe_xO: High resolution electrochemical measurements using zirconia solid electrolytes from 900–1400 K. Geochimica et Cosmochimica Acta, 50, 2439–2452.

Hsu, L.C. (1968) Selected phase relationships in the system Al-Mn-Fe-Si-O-H: A model for garnet equilibria. Journal of Petrology, 9, 40–83.

Karpinskaya, T.B., Ostrovsky, I.A., and Yevstigneeva, T.L. (1982) Synthetic pure iron skiagite garnet. Izvestia Akademie Nauk, SSSR, 9, 128–129 (in Russian).

Keesman, I., Matthes, S., Schreyer, W., and Seifert, F. (1971) Stability of almandine in the system FeO-(Fe_2O_3)-Al_2O_3-SiO_2-(H_2O) at elevated pressures. Contributions to Mineralogy and Petrology, 31, 132–144.

Kress, V.C., and Carmichael, I.S.E. (1988) Stoichiometry of the iron oxidation reaction in silicate melts. American Mineralogist, 73, 1267–1274.

Lattard, D., and Schreyer, W. (1983) Synthesis and stability of the garnet calderite in the system Fe-Mn-Si-O. Contributions to Mineralogy and Petrology, 84, 199–214.

Lucas, H., Muggeridge, M.T., and McConchie, D.M. (1989) Iron in kimberlitic ilmenites and chromian spinels: A survey of analytical techniques. In J. Ross, Ed., Kimberlites and related rocks, vol. 2, p. 311–319. Geological Society of Australia Special Publication, Blackwell, Australia.

Luth, R.W., Virgo, D., Boyd, F.R., and Wood, B.J. (1990) Ferric iron in mantle-derived garnets, implications for thermobarometry and for the oxidation state of the mantle. Contributions to Mineralogy and Petrology, 104, 56–72.

Massalski, T.B., Murray, J.L., Bennett, L.H., and Baker, H. (1986) Binary alloy phase diagrams, p. 24–26. American Society for Metals, Metals Park, Ohio.

Meagher, E.P. (1980) Silicate garnets. In Mineralogical Society of America Reviews in Mineralogy, 5, 25–66.

Novak, G.A., and Gibbs, G.V. (1971) The crystal chemistry of the silicate garnets. American Mineralogist, 56, 791–825.

O'Neill, H.St.C. (1987) Quartz-fayalite-iron and quartz-fayalite-magnetite equilibria and the free energy of formation of fayalite (Fe_2SiO_4) and magnetite (Fe_3O_4). American Mineralogist, 72, 67–75.

O'Neill, H.St.C., and Navrotsky, A. (1984) Cation and thermodynamic properties of binary spinel solid solutions. American Mineralogist, 68, 181–194.

O'Neill, H., and Wood, B. (1979) An experimental study of Fe-Mg partitioning between garnet and olivine and its calibration as a geothermometer. Contributions to Mineralogy and Petrology, 70, 59–70.

O'Neill, H.St.C., Rubie, D.C., Canil, D., Geiger, C.A., Ross, C.R., II, Seifert, F., and Woodland, A.B. (1993) Ferric iron in the upper mantle and in transition zone assemblages: Implications for relative oxygen fugacities in the mantle. In E. Takahashi, R. Jeanloz, and D. Rubie, Eds., Evolution of the Earth and planets: AGU monograph vol. 74 and IUGG vol. 14, p. 73–88. American Geophysical Union, Washington, DC.

Paladino, A.E., and Maguire, E.A. (1970) Microstructure development in yttrium iron garnet. Journal of the American Ceramic Society, 53, 98–102.

Ringwood, A.E. (1975) Composition and petrology of the Earth's mantle, 618 p. McGraw-Hill, New York.

Robie, R.A., Hemingway, B.S., and Fisher, J.R. (1978) Thermodynamic properties of minerals and related substances at 298.15 K and 1 bar (10^5 Pa) pressure and at higher temperature. U.S. Geological Survey Bulletin 1452, 456 p.

Ross, N., and Navrotsky, A. (1987) The Mg_2GeO_4 olivine-spinel phase transition. Physics and Chemistry of Minerals, 14, 473–481.

Ross, N., Akaogi, M., Navrotsky, A., Susaki, J., and McMillan, P. (1986) Phase transitions among the $CaGeO_3$ polymorphs (wollastonite, garnet, and perovskite structures): Studies by high pressure synthesis, high temperature calorimetry, and vibrational spectroscopy and calculation. Journal of Geophysical Research, 91, 4685–4696.

Roth, R.S., Dennis, J.R., and McMurdie, H.F. (1987) Phase diagrams for ceramists, vol. VI, p. 454–456. American Ceramic Society, Westerville, Ohio.

Rubinstein, C.B., and Barns, R.L. (1964) Crystallographic data for rare-earth aluminum garnets. American Mineralogist, 49, 1489–1490.

Schreyer, W., and Baller, Th. (1980) Calderite, $Mn_3^{2+}Fe_2^{3+}Si_3O_{12}$, a high pressure garnet. Proceedings of the IMA Meeting, Experimental Mineralogy, 16, 68–77.

Shannon, R.D. (1976) Revised effective ionic radii and systematic studies of interatomic distances in halides and chalcogenides. Acta Crystallographica, A32, 751–767.

Stadnik, Z.M. (1984) Electric field gradient calculations in rare-earth iron garnets. Journal of Physics and Chemistry of Solids, 45, 311–318.

Wood, B.J., Bryndzia, L.T., and Johnson, K.E. (1990) Mantle oxidation state and its relation to tectonic environment. Science, 248, 337–345.

Woodland, A.B., and Wood, B.J. (1989) Electrochemical measurement of the free energy of almandine ($Fe_3^{+2}Al_2Si_3O_{12}$) garnet. Geochimica et Cosmochimica Acta, 53, 2277–2282.

Yagi, T., and Akimoto, S. (1976) Direct determination of coesite-stishovite transition by in-situ X-ray measurements. Tectonophysics, 35, 259–270.

Yagi, T., Akaogi, M., Shimomura, O., Suzuki, T., and Akimoto, S. (1987) In-situ observation of the olivine spinel transformation in Fe_2SiO_4 using synchrotron radiation. Journal of Geophysical Research, 92, 6207–6213.

Yoder, H.S., and Keith, M.L. (1951) Complete substitution of aluminum for silicon: The system $3MnO\cdot Al_2O_3\cdot 3SiO_2$-$3Y_2O_3\cdot 5Al_2O_3$. American Mineralogist, 36, 519–533.

Manuscript received October 9, 1992
Manuscript accepted May 10, 1993